Manipulation of the interlayer exchange coupling in perpendicular magnetized thin films via tunable magnetic-layer and spacer thicknesses

Kang Wang, Lijuan Qian, See-Chen Ying, and Gang Xiao*
Department of Physics, Brown University, Providence, Rhode Island 02912, USA

(Received 15 June 2020; revised 5 October 2020; accepted 7 October 2020; published 20 October 2020)

In this work, we fabricated interlayer exchange-coupled magnetic thin films with ferromagnetic layers separated by a spacer layer. We investigated the dependencies of the sign and strength of the interlayer exchange coupling (IEC) and magnetic configurations on both the ferromagnetic layer thicknesses and the spacer thickness. The change of sign of the IEC between the ferromagnetic layers can occur for a thickness change of ferromagnetic layers by as small as approximately 0.1 nm. By comparison, a minimum of approximately 0.2 nm spacer thickness change is required for the same transformation. We attribute the ferromagnetic layer thickness dependence of the IEC to changes in thermal magnon excitations and quantum interferences inside ferromagnetic layers that affect interactions between the ferromagnetic layers and the spacer layer. Our experimental results suggest that the IEC modifications via changing the magnetic-layer thickness can be more efficient for magnetic memory and sensing applications.

DOI: 10.1103/PhysRevB.102.144430

I. INTRODUCTION

The interlayer exchange-coupled magnetic thin film is formed from multilayers where two adjacent ferromagnetic layers are coupled through a nonmagnetic spacer layer in between. The interlayer exchange coupling (IEC) is an indirect exchange interaction that originates from interactions between localized spins in ferromagnetic layers and the itinerant electrons in the spacer layer [1–3]. According to the Ruderman-Kittel-Kasuya-Yosida (RKKY) theory [1–3], this leads to either a ferromagnetic or antiferromagnetic coupling between the ferromagnetic layers, depending on the thickness of the nonmagnetic spacer. Both the IEC sign and strength have been found to have an oscillatory dependence on the spacer thickness [4–10].

In many previous studies, the effects of the ferromagnetic-layer properties on the IEC were generally ignored. However, several theoretical [7,11–14] and experimental [15–21] works suggest that the ferromagnetic-layer thicknesses and charge carriers can affect the spin asymmetry of reflection coefficients at interfaces between the ferromagnetic layers and the nonmagnetic spacer, thus having influences on quantum interferences in the nonmagnetic spacer layer. The effects of ferromagnetic-layer thicknesses on the IEC have been observed in both in-plane magnetized [16,18,20] and perpendicular magnetized [15,17,19,21] magnetic thin films and superlattices. Among these are magnetic thin films with different ferromagnetic layers such as metallic ferromagnets [16–20], diluted magnetic semiconductors [21], and repeating ferromagnetic layers [15]. The spacers in these magnetic thin films include metallic [16–18,20], semiconducting [21], and insulating [15,19] layers. Most of these works have shown that the ferromagnetic-layer thicknesses [16,18–20] as well as the temperature of film [21] can have an influence on the IEC. Other works reported that the dipole interactions between different layers in the repeating structure [15,17] can also have an influence on the IEC. Moreover, ion liquid gating processes have been used to modify magnetizations and the IEC in magnetic thin films [9,22]. The magnetization and IEC modifications were attributed to changes in carrier density at the Fermi surface [9,23,24].

Numerical calculations using a free-electron model have shown that the IEC also has an oscillatory dependence on magnetic-layer thicknesses [7,13]. This prediction has been experimentally demonstrated in studies of multilayers including Co/Cu/Co [18], Fe/Cr [16], and Fe/Au/Fe [20]. It was found that the dependence of the oscillation period on the ferromagnetic-layer thicknesses is stronger than the dependence on the spacer thickness. This suggests that it can be more efficient for modifications of the IEC through controlling ferromagnetic-layer thicknesses. However, in these studies [16,18,20], only oscillations in the IEC strength were reported while the IEC sign remains unchanged. Theoretically, one expects that both the IEC sign and strength can show a dependence on magnetic-layer thicknesses. As shown in this work, below, it is important to reduce the magnetic anisotropy of the ferromagnetic layers in the magnetic thin films to facilitate the observation of the sign change of the IEC.

In previous works, in-plane magnetized interlayer exchange-coupled magnetic thin films have been widely studied [4–8,16,18,20]. To be applied in either magnetic sensors or memory devices with increasing areal densities, it is essential to reduce the negative effect of the fringing stray field. One approach is to switch the in-plane anisotropy to perpendicular anisotropy for the ferromagnetic layers. The perpendicular magnetized magnetic thin films possess a higher thermal stability and a lower writing critical current density [25,26]. These are crucial for spintronic technologies.

*gang_xiao@brown.edu

 ©2020 American Physical Society

In magnetic thin films, the IEC, together with magnetic anisotropies of the ferromagnetic layers, determines the final magnetic configurations and their responses to external field and spin-transfer torques [27,28]. Energy-efficient manipulations of the IEC and magnetic configurations in perpendicular magnetized magnetic thin films are therefore of great significance for applications in ultrahigh-density magnetic sensors and memory devices [26,29–32].

In this work, we show experimental results for a study of both ferromagnetic-layer and the spacer-layer thickness dependencies of the IEC and magnetic configurations in a mostly perpendicular magnetized magnetic-multilayer structure. This work is complemented by characterizations of the effects of magnetic anisotropies on magnetic configurations in the magnetic-multilayer structure.

II. SAMPLE PREPARATION

For our study, we fabricated magnetic thin films with both variable ferromagnetic-layer thicknesses and the spacer layer thickness. The magnetic thin films have the structure of Ta(4.0)/MgO(1.6)/$Co_{40}Fe_{40}B_{20}$(t_{CoFeB})/Ta(t_{Ta})/$Co_{40}Fe_{40}B_{20}$(0.8t_{CoFeB})/MgO(1.6)/TaO_x(2.0) (numbers are layer thicknesses in nanometers) where the ratio of the top ferromagnetic-layer thickness to the bottom ferromagnetic-layer thickness remains constant and equals to 0.8. The magnetic thin films were deposited on thermally oxidized silicon wafers using a high-vacuum magnetron sputtering system. After deposition, we annealed samples in a high-vacuum chamber at 210 °C for 1 h with the application of a perpendicular magnetic field of approximately 0.4 T. In the magnetic-multilayer structure, the thinner top ferromagnetic layer has a perpendicular magnetic anisotropy, and the thicker bottom ferromagnetic layer has a weak in-plane anisotropy. Characterizations of magnetic anisotropies of ferromagnetic layers are shown in Sec. IV in detail. The bottom Ta(4.0) layer is the buffer layer and the top TaO_x(2.0) layer is the capping layer that prevents underlying layers from oxidization on exposure to the atmosphere. MgO layers are used to promote perpendicular magnetic anisotropies of adjacent $Co_{40}Fe_{40}B_{20}$ layers [33,34]. To vary $Co_{40}Fe_{40}B_{20}$ layer thicknesses and the Ta spacer thickness, we fabricated wedge-shaped $Co_{40}Fe_{40}B_{20}$ layers and the Ta spacer layer along any direction from the center of the substrate. The wedge-shaped layers were fabricated through placing substrates with an off-centered displacement relative to the sputter source while depositing multilayers. We also rotated substrates with a constant speed. After deposition, we patterned multilayers into Hall bars at different positions on samples. Through applying current along the long stripe of the Hall bar and detecting the Hall resistance R_H where the anomalous Hall resistance that is proportional to the perpendicular magnetization M_z is dominant [35,36], we can analyze magnetic configurations and the IEC as functions of both $Co_{40}Fe_{40}B_{20}$ layer thicknesses and the Ta spacer thickness.

III. CHARACTERIZATIONS ON FILM THICKNESSES

To determine the $Co_{40}Fe_{40}B_{20}$ layer thickness and the Ta spacer thickness at different positions on samples, we first

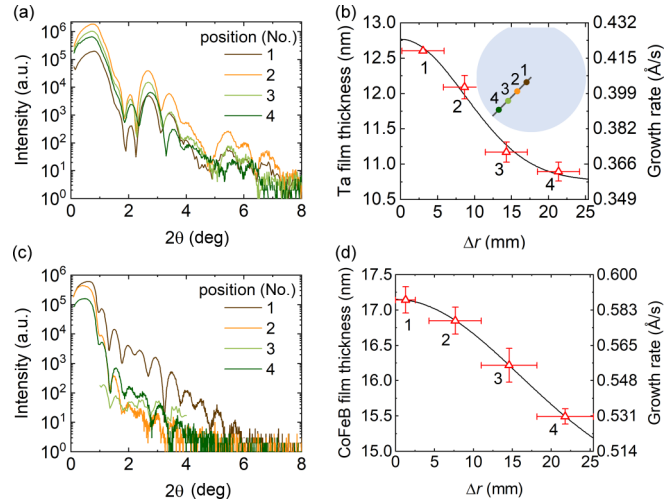

FIG. 1. (a) X-ray reflection measurements at four different positions of a Ta film that was deposited in 300.9 s. Four illumination positions are schematically presented in the inset in (b). (b) Ta film thicknesses and growth rates at different radial positions, obtained from x-ray reflection measurements. Δr is the radial distance between the illumination point and the center of the silicon wafer. (c) X-ray reflection measurements at four different positions of a $Co_{40}Fe_{40}B_{20}$ film that was deposited in 291.8 s. (d) $Co_{40}Fe_{40}B_{20}$ film thicknesses and growth rates at different radial positions, obtained from x-ray reflection measurements. Error bars were derived from the measurements and uncertainty of illumination positions.

deposited a thicker $Co_{40}Fe_{40}B_{20}$ film and a Ta film on thermally oxidized silicon wafers. We then measured film thicknesses and corresponding growth rates at different positions through high-resolution x-ray reflection (XRR) measurements. We chose four points with different radial distances Δr from the center of the substrate, as schematically presented in the inset in Fig. 1(b). The XRR results for Ta and $Co_{40}Fe_{40}B_{20}$ films are respectively presented in Figs. 1(a) and 1(c). We calculated film thicknesses through $\frac{\lambda}{2\Delta\theta}$ where $\lambda = 1.54$ Å is the x-ray wavelength and $\Delta\theta$ is the period of oscillations. The corresponding growth rate is then given by $\frac{\lambda}{2t\Delta\theta}$ where t is the deposition time for films. Film thicknesses and growth rates for Ta and $Co_{40}Fe_{40}B_{20}$ are respectively presented in Figs. 1(b) and 1(d). As shown in Figs. 1(b) and 1(d), the growth rates for both Ta and $Co_{40}Fe_{40}B_{20}$ decrease when increasing the radial distance Δr from the center of the substrate. The Ta film thickness shows an average 0.75% change per millimeter, and the $Co_{40}Fe_{40}B_{20}$ film thickness shows an average 0.77% change per millimeter. Error bars of the thickness estimation were derived from error bars of the period of oscillations. The horizontal error bars were derived from the uncertainty of illumination positions. The error bars of the film thickness estimation for both Ta and $Co_{40}Fe_{40}B_{20}$ are smaller than ±0.25 nm. In Supplemental Material Note 2 [37], we show that both films have rather smooth surfaces with the surface roughness smaller than 0.5 nm, derived from the atomic-force microscopy measurement and the fitting of XRR results. The small error bars of the film thickness estimation together with small values of the film surface roughness suggest that the layer

thicknesses in the multilayer structure are well defined. We have also performed the atomic-force microscopy measurement for a multilayer sample [37]. The result again shows the smooth surface with the surface roughness as small as 0.1 nm. This is an indication of the high quality of the multilayer sample with small interface roughness, which can be also confirmed from the XRR measurement on the multilayer stack [37]. The knowledge of film thicknesses and growth rates at different positions on samples allows us to know exactly and control layer thicknesses in the magnetic-multilayer structure through controlling deposition times for different layers.

IV. MAGNETIC ANISOTROPIES OF FERROMAGNETIC LAYERS

The magnetic configuration in the magnetic-multilayer structure is determined by the minimization of the free energy including the Zeeman, anisotropy, and IEC energy terms,

$$\begin{aligned} E_{\rm tot} = &-\mu_0(0.8M_{\rm S,\,top}t_{\rm CoFeB}\boldsymbol{H}_{\rm ext}\cdot\boldsymbol{m}_{\rm top} \\ &+M_{\rm S,\,bottom}t_{\rm CoFeB}\boldsymbol{H}_{\rm ext}\cdot\boldsymbol{m}_{\rm bottom}) \\ &-0.8K_{\rm u,top}t_{\rm CoFeB}(\boldsymbol{m}_{\rm top}\cdot\boldsymbol{e}_{\rm z})^2 \\ &-K_{\rm u,bottom}t_{\rm CoFeB}(\boldsymbol{m}_{\rm bottom}\cdot\boldsymbol{e}_{\rm z})^2+J_{\rm IEC}(\boldsymbol{m}_1\cdot\boldsymbol{m}_2). \end{aligned} \quad (1)$$

In this equation, μ_0 is the vacuum permeability and $\boldsymbol{H}_{\rm ext}$ is the external magnetic field. $M_{\rm S}$, $\boldsymbol{m}$, and $K_{\rm u}$ are the saturation magnetization, normalized magnetization vector, and magnetic anisotropy, respectively. Subscripts "top" and "bottom" refer to parameters of the top and bottom ferromagnetic layers, respectively. $\boldsymbol{e}_{\rm z}$ is the normalized vector along the z axis that is the direction normal to the layers. Here we note that, in this free energy expression, a positive value of $K_{\rm u}$ (perpendicular magnetic anisotropy) favors a magnetization for the corresponding layer along the normal direction and a negative value of $K_{\rm u}$ (in-plane anisotropy) favors a magnetization perpendicular to the normal. The fourth term on the right-hand side is the IEC energy term. A positive IEC energy coefficient $J_{\rm IEC}$ (antiferromagnetic IEC) favors an antiferromagnetic configuration of the magnetization in the two ferromagnetic layers while a negative $J_{\rm IEC}$ (ferromagnetic IEC) favors a ferromagnetic configuration. However, the resultant magnetic configuration in the two layers can be noncollinear and not necessarily parallel or antiparallel. It depends on the interplay of different terms in the free energy consisting of magnetic anisotropies of the two ferromagnetic layers, the IEC, as well as the external magnetic field $\boldsymbol{H}_{\rm ext}$.

In this section, we study the magnetic anisotropies of the two ferromagnetic layers in the magnetic-multilayer structure. For this purpose, we fabricated two structures consisting of multilayers of Ta($t_{\rm Ta,top}$)/$Co_{40}Fe_{40}B_{20}$($0.8t_{\rm CoFeB}$)/MgO(1.6)/TaO_x(2.0) and MgO(1.6)/$Co_{40}Fe_{40}B_{20}$($t_{\rm CoFeB}$)/Ta($t_{\rm Ta,bottom}$) that have the same structure as the top and bottom ferromagnetic layers, respectively, in the multilayer structure that we fabricated to study the effect of IEC. In the following, we refer to the two structures as "the top structure" and "the bottom structure," respectively. The sample growth and fabrication procedures are the same as that described in Sec. II.

Figures 2(a) and 2(b) show the results for the Hall resistance $R_{\rm H}$ versus perpendicular magnetic field $H_{\rm z}$ for the

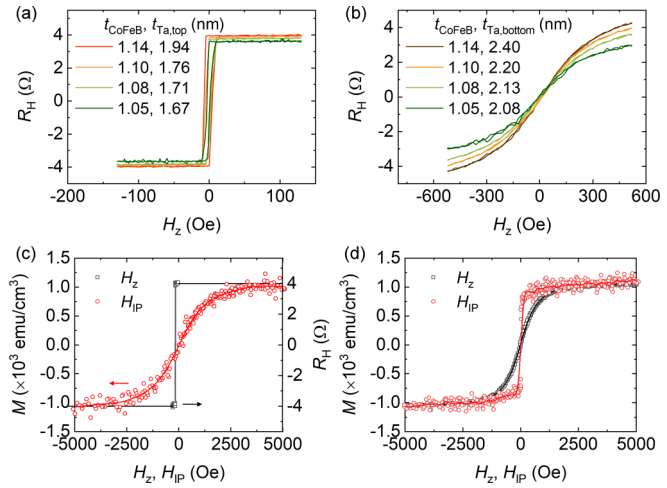

FIG. 2. (a) Hall resistance measurement for the structure of Ta($t_{\rm Ta,top}$)/$Co_{40}Fe_{40}B_{20}$($0.8t_{\rm CoFeB}$)/MgO(1.6)/TaO_x(2.0) (top structure). The results were measured through Hall bars located at different positions on the sample with different Ta($t_{\rm Ta,top}$) and $Co_{40}Fe_{40}B_{20}$($0.8t_{\rm CoFeB}$) layer thicknesses. (b) Hall resistance measurement for the structure of MgO(1.6)/$Co_{40}Fe_{40}B_{20}$ ($t_{\rm CoFeB}$)/Ta($t_{\rm Ta,bottom}$) (bottom structure). The results were measured through Hall bars located at different positions on the sample with different Ta($t_{\rm Ta,bottom}$) and $Co_{40}Fe_{40}B_{20}$($t_{\rm CoFeB}$) layer thicknesses. (c) The magnetization measurement (red circle dots) and the Hall resistance measurement (black square dots) with applications of the in-plane magnetic field $H_{\rm IP}$ and the perpendicular magnetic field $H_{\rm z}$, respectively, for the top structure. (d) The magnetization measurement with applications of the in-plane magnetic field $H_{\rm IP}$ (red circle dots) and the perpendicular field $H_{\rm z}$ (black square dots), for the bottom structure. In (c) and (d), dots are experimental results and lines are to guide the eye.

top structure and the bottom structure, respectively. The Hall resistance were measured through Hall bars located at different positions on the two samples. Figure 2(a) shows an almost constant value of $R_{\rm H}$ with the same sign as the applied field $H_{\rm z}$ for the top structure. As the field $H_{\rm z}$ switches sign, there is also a rapid switching of the sign of the Hall resistance. This implies that the top structure has a perpendicular magnetic anisotropy leading to a saturated magnetization lining along the direction of the external field $H_{\rm z}$ with a rapid switching around the zero magnetic field. On the other hand, for the bottom structure, Fig. 2(b) shows a smooth curve for the Hall resistance $R_{\rm H}$ that vanishes at zero field and smoothly increases or decreases with the external field $H_{\rm z}$ until saturation. This indicates that the bottom structure has an in-plane anisotropy such that the magnetization lies in-plane at $H_{\rm z}=0$. The magnetization gradually gets tilted out of the plane with a finite value of $H_{\rm z}$, eventually aligning with $H_{\rm z}$ at a large magnetic field. For both structures, the behavior of the Hall resistance versus $H_{\rm z}$ changes only slightly as the ferromagnetic-layer thickness is changed in the range from 1.05 to 1.14 nm, measured at different positions on samples. This implies that there are little variations in magnetic anisotropies of the top and bottom ferromagnetic layers in the magnetic-multilayer structure as the ferromagnetic-layer thickness $t_{\rm CoFeB}$ is varied in the range corresponding to

our following studies on the influence of ferromagnetic-layer thicknesses on the IEC. The magnetic anisotropy of ferromagnetic layers dominantly originates from the interface between the MgO layer and the $Co_{40}Fe_{40}B_{20}$ layer [34,38]. The Ta layer thickness in the range from 1.0 to 2.4 nm in our studies therefore should have little effect on magnetic anisotropies of the two ferromagnetic layers.

For further support of the above interpretation of the Hall resistance results and to quantify magnetic anisotropies of the two structures, we have measured both the in-plane and perpendicular components of the magnetization M as functions of applied perpendicular magnetic field H_z and in-plane magnetic field H_{IP} through a vibrating-sample magnetometer. The results for the top structure and for the bottom structure are respectively presented in Figs. 2(c) and 2(d). The results were all measured for samples located near the center of the wafer. The effective magnetic anisotropy values can then be derived through the area between curves of the magnetization versus the perpendicular and the in-plane magnetic field. For the top structure, the anisotropy $K_{u,top}$ is obtained to be 1.29×10^5 J/m^3, and for the bottom structure, the anisotropy $K_{u,bottom}$ is obtained to be -4.21×10^4 J/m^3. The smaller value of the negative anisotropy for the bottom structure suggests that the in-plane anisotropy of the bottom structure is relatively weak.

V. DEPENDENCE OF MAGNETIC CONFIGURATIONS ON THE SPACER AND FERROMAGNETIC-LAYER THICKNESSES

With the knowledge of magnetic anisotropies of the two ferromagnetic layers, we then study the combined effect of IEC and magnetic anisotropies on magnetic configurations in the magnetic-multilayer structure. In particular, we focus on how the IEC changes as a function of the spacer layer and ferromagnetic-layer thicknesses. Figure 3(a) shows the schematic of the Hall bar that was used to measure Hall resistance R_H of samples. Figure 3(b) shows the Hall resistance of a magnetic-multilayer structure with $t_{Ta} = 1.61$ nm, as a function of the perpendicular magnetic field H_z. The Hall bar that was used to measure the Hall resistance is located near the center of the sample where $t_{CoFeB} = 1.12$ nm. There is a plateau in the region around zero magnetic field that forms a loop on increasing or decreasing the perpendicular magnetic field H_z. On further increasing or decreasing the external field, a slanted curve appears in the intermediate field region. The slanted curve eventually saturates at a higher magnetic field where both layers are aligned in the direction of the external field. This gradual transformation of the intermediate state into the final saturated parallel state is referred to as the spin-flop transition.

The result for the Hall resistance as shown in Fig. 3(b) can be interpreted as follows. For this set of parameters of t_{Ta} and t_{CoFeB}, $J_{IEC} > 0$ (antiferromagnetic IEC). The antiferromagnetic IEC would favor the top- and bottom-layer magnetizations to point in opposite directions to lower the free energy. However, as shown in Sec. IV, the top layer has a perpendicular magnetic anisotropy and the bottom layer a weaker in-plane anisotropy. The combined effect of the antiferromagnetic IEC and anisotropies of the two ferromagnetic

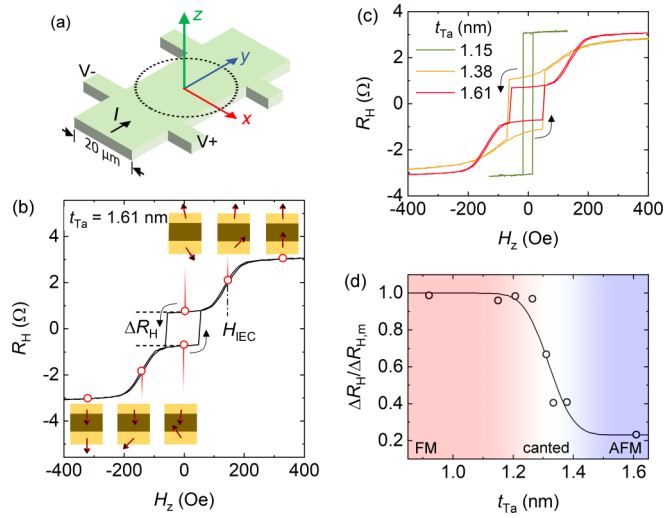

FIG. 3. (a) The schematic of the Hall bar structure. (b) Hall resistance R_H vs perpendicular magnetic field H_z for a magnetic-multilayer structure with $t_{Ta} = 1.61$ nm and $t_{CoFeB} = 1.12$ nm. The inserts show schematics of magnetic configurations at different perpendicular magnetic fields. ΔR_H is the difference between Hall resistances for two opposite spin states at zero magnetic field. (c) Hall resistance R_H vs perpendicular magnetic field H_z for magnetic multilayers with different t_{Ta} and with the same ferromagnetic layer thickness of $t_{CoFeB} = 1.12$ nm. (d), $\Delta R_H/\Delta R_{H,m}$ as a function of t_{Ta}. Dots are experimental data and the line is a guide for the eyes. Arrows in (b) and (c) represent switching directions.

layers would lead to canted magnetization in both layers. The degree of canting of the magnetization for each layer results from the interplay of the IEC and magnetic anisotropy. The top layer with a stronger perpendicular anisotropy should have a magnetization that is pointed mainly along the normal direction with a small in-plane component. On the other hand, the bottom-layer magnetization should be more canted with a larger in-plane component due to its weaker in-plane anisotropy competing against an antiferromagnetic IEC with the top layer. These qualitative consideration remains true in the presence of a weak external field H_z. In Supplemental Material Note 1 [37], we show that the in-plane anisotropy of the bottom ferromagnetic layer is actually an easy-axis scenario with a rather weak anisotropy perpendicular to the direction of the ferromagnetic-layer thickness gradient. This weak easy-axis anisotropy may have an effect on the in-plane magnetization direction in the magnetic-multilayer structure.

The spin-flop transition at higher external field H_z originates from the competition between the IEC energy, the Zeeman energy from the external magnetic field, and the anisotropy energy for the flipping of the normal component of the magnetization of the bottom layer from pointing against the external field to pointing along the external field. In a region where the IEC and Zeeman energy dominate over the weak anisotropy of the bottom layer, we can estimate the IEC strength by balancing the Zeeman energy against the IEC. Denoting the external field at the center position of the S-shaped spin-flop transition curve as the exchange coupling field H_{IEC}, this yields an estimate for the IEC

strength as

$$|J_{\mathrm{IEC}}| = \mu_0 H_{\mathrm{IEC}} M_{\mathrm{S}} t_{\mathrm{FM}}, \tag{2}$$

where $M_{\mathrm{S}} = 1.06 \times 10^6$ A/m is the saturation magnetization measured through a vibrating-sample magnetometer, and $t_{\mathrm{FM}} = 0.9 t_{\mathrm{CoFeB}} = 1.0$ nm is the average of two ferromagnetic-layer thicknesses. For the multilayer structure with $t_{\mathrm{Ta}} = 1.61$ nm, H_{IEC} is determined to be 140.6 Oe and the IEC strength is estimated to be 0.0149 mJ/m^2. This IEC strength is comparable to the previous report of magnetic multilayers with the Ta spacer [8,39]. Note that this estimate breaks down near a region where IEC changes sign where the magnitude of IEC no longer dominates over the anisotropy energy.

We then measured Hall resistance of magnetic multilayers with different Ta spacer thicknesses but the same $Co_{40}Fe_{40}B_{20}$ layer thickness of $t_{\mathrm{CoFeB}} = 1.12$ nm, as shown in Fig. 3(c). All the results were measured through Hall bars located near the center of samples. We controlled the deposition time for $Co_{40}Fe_{40}B_{20}$ layers the same for each sample, while we varied the deposition time for the Ta spacer for different samples. When decreasing t_{Ta} from 1.61 to 1.38 nm, the plateau in the region around zero magnetic field becomes slanted. We interpret this effect as originating from a decrease in the antiferromagnetic IEC strength. In this case, the weak magnetic anisotropy in the thicker bottom ferromagnetic layer plays a more important role in leading to a more canted magnetization structure with a larger in-plane component of the bottom-layer magnetization. This gives rise to a larger value of ΔR_{H} that is the difference of Hall resistances R_{H} for two opposite spin states at zero magnetic field. On further decreasing t_{Ta} to 1.15 nm, only a square loop is present. We interpret this as due to the fact that the IEC between the two ferromagnetic layers has changed sign changing from an antiferromagnetic to a ferromagnetic IEC. The anisotropy term for the bottom layer plays a minor role when the top and bottom layers are ferromagnetically coupled. When decreasing the perpendicular magnetic field from the positive saturation field to zero field, or increasing the perpendicular field from the negative saturation field to zero field, magnetizations in both $Co_{40}Fe_{40}B_{20}$ layers remain aligned along the external field direction, in order to lower both the IEC energy and the Zeeman energy from the external magnetic field. This leads to a loop with a narrow width and a ΔR_{H} value which is very close to $\Delta R_{\mathrm{H,m}}$ that is defined as the difference of Hall resistances R_{H} for two opposite spin states at saturation fields. Based on this interpretation, we can then use the value of $\Delta R_{\mathrm{H}}/\Delta R_{\mathrm{H,m}}$ as a qualitative measure of both the sign and strength of the IEC between the two ferromagnetic layers. A small value of $\Delta R_{\mathrm{H}}/\Delta R_{\mathrm{H,m}}$ would correspond to an antiferromagnetic IEC and a large value to a ferromagnetic IEC. Figure 3(d) shows $\Delta R_{\mathrm{H}}/\Delta R_{\mathrm{H,m}}$ as a function of t_{Ta}. $\Delta R_{\mathrm{H}}/\Delta R_{\mathrm{H,m}}$ increases steadily as the Ta spacer thickness changes from 1.5 to 1.2 nm. It is hard to determine the critical thickness at which the IEC sign reverses. However, we can estimate through Fig. 3(d) that the sign reversal occurs around $\Delta R_{\mathrm{H}}/\Delta R_{\mathrm{H,m}} = 0.5$ or around $t_{\mathrm{Ta}} = 1.3$ nm. At zero field, the antiparallel magnetization of the ferromagnetic layers transforms into parallel magnetization as the spacer thickness changes by approximately 0.2 nm. This change of magnitude and sign of the IEC with the Ta spacer thickness corresponds to the well-established oscillatory behavior of the RKKY interaction [1–3].

With the above understanding of the dependence of the Hall resistance on the interplay of magnetic anisotropies, the IEC and the external field, we then proceed to measure the Hall resistance through Hall bars at different positions on samples to map both $Co_{40}Fe_{40}B_{20}$ layer thicknesses and the Ta spacer thickness dependences of magnetic configurations. Figure 4(a) shows Hall loops of Hall bars at different positions in a single batch. Position (i) is near the center of the sample. Positions (ii) and (iii) are respectively located at a position with an intermediate radial distance Δr, and near the edge of the sample. There is a qualitative change of the Hall resistance curve from the plateau plus a spin-flop transition at position (i) to the very narrow square loop at position (iii), indicating a change of sign and strength of IEC as the thicknesses of the ferromagnetic and spacer layers are varied. Figure 4(b) shows that the radial distance Δr dependences of ΔR_{H} and $\Delta R_{\mathrm{H,m}}$. $\Delta R_{\mathrm{H,m}}$ increases slightly as the radial distance Δr increases, because of both decreases in $Co_{40}Fe_{40}B_{20}$ layer thicknesses and the Ta spacer thickness. In addition, ΔR_{H} increases gradually as the radial distance Δr increases, implying the gradual changes in the IEC along the radial direction.

We then performed Hall resistance measurements on different samples, and plotted $\Delta R_{\mathrm{H}}/\Delta R_{\mathrm{H,m}}$ as functions of both $Co_{40}Fe_{40}B_{20}$ layer thicknesses and the Ta spacer thickness. All the results are presented in Fig. 4(c) where crosses and circles indicate corresponding $Co_{40}Fe_{40}B_{20}$ layer thicknesses and the Ta spacer thickness of magnetic multilayers at different positions where Hall bars locate. The totality of all the data shows that the magnetic configurations not only depend on the Ta spacer thickness, but also depend on $Co_{40}Fe_{40}B_{20}$ layer thicknesses. This figure serves as a phase diagram indicating where the IEC is ferromagnetic (colored in red) and where the IEC is antiferromagnetic (colored in blue), and the boundary between the two types of coupling where the IEC is vanishingly small. In Fig. 4(d), we plotted $\Delta R_{\mathrm{H}}/\Delta R_{\mathrm{H,m}}$ as a function of the $Co_{40}Fe_{40}B_{20}$ layer thickness where the data are collected for samples with the Ta thickness in the 1.30–1.55-nm range. This figure shows that for magnetic multilayers with the Ta spacer thickness around 1.4 nm, when decreasing $Co_{40}Fe_{40}B_{20}$ layer thickness t_{CoFeB} from a thickness of about 1.12 nm, the strength of the antiferromagnetic IEC starts to decrease until it vanishes at a $Co_{40}Fe_{40}B_{20}$ layer thickness of about 1.07 nm. As the ferromagnetic-layer thickness is decreased further, the ferromagnetic IEC strength increases continuously.

According to our previous discussions of the role of anisotropy energy, it can have an influence on the Hall resistance behavior versus the external field [40,41]. However, we can exclude the possibility that the qualitative change of $\Delta R_{\mathrm{H}}/\Delta R_{\mathrm{H,m}}$ as a function of the thickness of the ferromagnetic layer in our studies is due to the anisotropy effect. First, in Sec. IV, we have concluded from the experimental data shown in Fig. 2 that there are little variations in the magnetic anisotropies of ferromagnetic layers when the ferromagnetic-layer thickness t_{CoFeB} is varied in the range in the studies shown in Fig. 4. In addition, a large anisotropy variation would also cause changes in the saturation field [40,41] at which the Hall resistance reaches its maximum

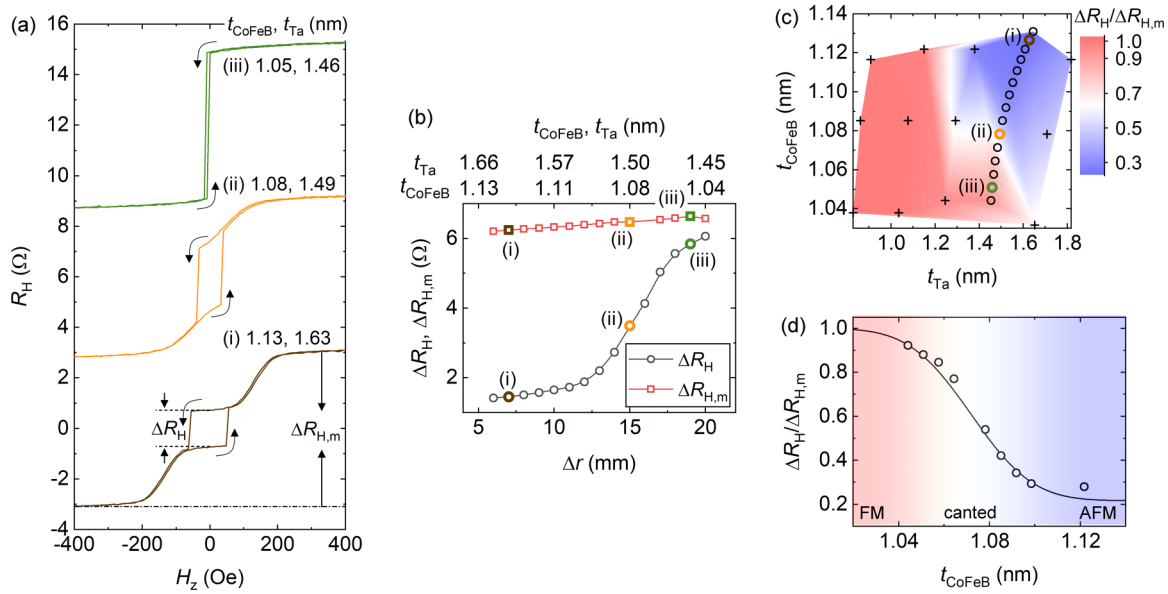

FIG. 4. (a) Hall resistance R_H vs perpendicular magnetic field H_z for Hall bars at different positions in a single batch. $\Delta R_{H,m}$ is the difference between Hall resistances for two opposite spin states at positive and negative saturation fields. (b) ΔR_H and $\Delta R_{H,m}$ as a function of the radial distance Δr in a single batch. The data correspond to the array of circles in (c). In (b), labels of t_{Ta} and t_{CoFeB} are also given. (c) Phase diagram of $\Delta R_H/\Delta R_{H,m}$ as functions of both Ta spacer thickness t_{Ta} and the $Co_{40}Fe_{40}B_{20}$ layer thickness t_{CoFeB}. Crosses and circles indicate corresponding t_{Ta} and t_{CoFeB} of magnetic multilayers at different positions where Hall bars locate. Circles correspond to the data in (b). The blue area refers to the antiparallel magnetization of the ferromagnetic layers, and the red area refers to the parallel magnetization of the ferromagnetic layers. The area with light colors refers to the canted magnetization state. (d) $\Delta R_H/\Delta R_{H,m}$ as a function of t_{CoFeB}. The data are collected for samples with t_{Ta} in the 1.3–1.55-nm range. Arrows in (a) represent switching directions.

value with both layers having magnetizations pointed along the direction of the external magnetic field. This has not been observed as shown clearly from the data shown in Fig. 4(a). All these observations support our interpretation that the qualitative change of the Hall resistance $\Delta R_H/\Delta R_{H,m}$ shown in Fig. 4 corresponds of the change of both the sign and magnitude of the IEC as a function of both the spacer layer and ferromagnetic-layer thicknesses.

VI. DISCUSSIONS AND CONCLUSIONS

Observations of the effects of ferromagnetic layers on the IEC in our magnetic multilayers are expected, because of both the weak IEC strength and the weak magnetic anisotropy in the thicker bottom ferromagnetic layer. Magnetic configurations in magnetic thin films are determined by competitions between the IEC energy and the magnetic anisotropy energy. The weak magnetic anisotropy energy in the bottom layer in our multilayer structure makes it possible to observe changes in Hall resistance measurement even when the IEC has a minor change.

Varying ferromagnetic-layer thicknesses induces changes in both thermal magnon excitations and quantum interferences inside the ferromagnetic layers. On the one hand, the decrease in $Co_{40}Fe_{40}B_{20}$ layer thicknesses weakens the IEC strength, because thermal magnetic fluctuations increase and thermal magnon excitations become more important in reduction of the IEC strength [42,43]. On the other hand, varying ferromagnetic-layer thicknesses also tunes quantum interferences inside the ferromagnetic layers [7,13], thus affecting spin asymmetry of reflection coefficients at interfaces which affect quantum interferences in the Ta spacer. The film quality and interface roughness can also affect spin asymmetry of reflection coefficients at interfaces, giving rise to the IEC variation. However, here we confirm that the IEC variation in our studies is most probably the result of thickness change itself, and no obvious spatial variations in the interface roughness, crystalline structures, and compositions of the deposited $Co_{40}Fe_{40}B_{20}$ has been observed in the atomic-force microscopy, XRR, transport, and energy dispersive x-ray spectroscopy measurements [37].

Most interestingly, as shown in Figs. 4(c) and 4(d), the IEC changes sign when ferromagnetic-layer thicknesses change by as small as approximately 0.1 nm. This value is smaller than the Ta spacer thickness change [approximately 0.2 nm, Fig. 3(d)] for the same transformation, suggesting that it is more efficient to modify the IEC by varying ferromagnetic-layer thicknesses.

Varying the deposition time is one way to tune the ferromagnetic-layer thicknesses. One expects that using other external controls such as voltage controls [9,22] and optics [44,45] can also manipulate the layer thicknesses, as well as charge carriers in the ferromagnetic layers, thus manipulating the IEC between the ferromagnetic layers. This manipulation is expected to have a lower energy-consumption, compared with the manipulation via tunning the spacer properties. If the IEC sign reversal is achieved via external controls, the energy-efficient switching between different magnetic configurations would be realized which is desirable for magnetic memory applications.

For magnetic sensing applications, the magnetoresistive response and/or the Hall voltage response to the external field

should be reversible and with the zero coercivity [31,32,46]. Besides magnetoresistive sensors [46], a high-performing anomalous Hall sensor based on the interlayer-exchange coupled magnetic thin film has been also reported recently [31]. In these sensors, in addition to magnetic anisotropies, the IEC provides a handle to control their responses to the external field, thus controlling their sensing capability including the sensitivity and the dynamic range. The more sensitive response of the IEC to the ferromagnetic-layer properties can lead manipulations of the sensing performance of magnetic sensors to be more energy efficient by controlling the ferromagnetic-layer properties via different methods including the external controls as stated previously.

Although critical thicknesses for the IEC sign reversal may be different for different magnetic-multilayer systems, we expect that the efficient manipulations of the IEC via magnetic-layer effects would be consistent, which remains to be further studied. Especially when the spacer thickness is around the value at which the IEC sign reversal occurs, the energy-efficient manipulations of both the IEC sign and strength can be achieved.

In conclusion, we have fabricated perpendicular magnetized magnetic thin films with the structure of Ta(4.0)/MgO(1.6)/$Co_{40}Fe_{40}B_{20}$(t_{CoFeB})/Ta(t_{Ta})/$Co_{40}Fe_{40}B_{20}$(0.8t_{CoFeB})/MgO(1.6)/TaO_x(2.0), and studied the dependences of the IEC and magnetic configurations on both the $Co_{40}Fe_{40}B_{20}$ layer thicknesses and the Ta spacer thickness. It is found that the $Co_{40}Fe_{40}B_{20}$ layer thicknesses influence both the IEC sign and strength. Compared to the Ta spacer thickness change (approximately 0.2 nm) required for the sign change of the IEC, we found that the same transformation occurs when the $Co_{40}Fe_{40}B_{20}$ layer thicknesses change by as small as approximately 0.1 nm. This suggests that a more energy-efficient manipulation of the IEC can be achieved by considering magnetic-layer effects which were generally ignored. Our studies provide a guide to future explorations on energy-efficient manipulations of the IEC via controlling magnetic-layer properties such as controlling the magnetic moments, magnon excitations, or topology of the Fermi surface.

ACKNOWLEDGMENT

The work was supported by National Science Foundation (NSF) under Grant No. OMA-1936221.

[1] T. Kasuya, Prog. Theor. Exp. Phys. **16**, 45 (1956).
[2] M. A. Ruderman and C. Kittel, Phys. Rev. **96**, 99 (1954).
[3] K. Yosida, Phys. Rev. **106**, 893 (1957).
[4] Z. Q. Qiu, J. Pearson, and S. D. Bader, Phys. Rev. B **46**, 8659 (1992).
[5] Z. Q. Qiu, J. Pearson, A. Berger, and S. D. Bader, Phys. Rev. Lett. **68**, 1398 (1992).
[6] P. Bruno, Phys. Rev. B **52**, 411 (1995).
[7] J. Barnaś, J. Magn. Magn. Mater. **111**, L215 (1992).
[8] S. S. P. Parkin, Phys. Rev. Lett. **67**, 3598 (1991).
[9] Q. Yang, L. Wang, Z. Zhou, L. Wang, Y. Zhang, S. Zhao, G. Dong, Y. Cheng, T. Min, Z. Hu, W. Chen, K. Xia, and M. Liu, Nat. Commun. **9**, 991 (2018).
[10] Z. Kurant, M. Tekielak, I. Sveklo, A. Wawro, and A. Maziewski, J. Magn. Magn. Mater. **475**, 683 (2019).
[11] C.-H. Chang, K.-P. Dou, Y.-C. Chen, T.-M. Hong, and C.-C. Kaun, Sci. Rep. **5**, 16844 (2015).
[12] S. Blizak, G. Bihlmayer, S. Blügel, and S. E. H. Abaidia, Phys. Rev. B **91**, 014408 (2015).
[13] P. Bruno, Europhys. Lett. **23**, 615 (1993).
[14] M. Stier and W. Nolting, Phys. Rev. B **84**, 094417 (2011).
[15] L. Li, D. Han, W. Lei, Z. Liu, F. Zhang, X. Mao, P. Wang, and H. Hou, J. Appl. Phys. **116**, 123904 (2014).
[16] S. N. Okuno and K. Inomata, Phys. Rev. Lett. **72**, 1553 (1994).
[17] Z. Liu, F. Zhang, B. Xu, D. Yu, J. He, and Y. Tian, J. Phys. D: Appl. Phys. **42**, 035010 (2009).
[18] P. J. H. Bloemen, M. T. Johnson, M. T. H. van de Vorst, R. Coehoorn, J. J. de Vries, R. Jungblut, J. aan de Stegge, A. Reinders, and W. J. M. de Jonge, Phys. Rev. Lett. **72**, 764 (1994).
[19] L. E. Nistor, B. Rodmacq, S. Auffret, A. Schuhl, M. Chshiev, and B. Dieny, Phys. Rev. B **81**, 220407(R) (2010).
[20] S. N. Okuno and K. Inomata, Phys. Rev. B **51**, 6139 (1995).
[21] P. Chongthanaphisut, S.-K. Bac, S. Choi, K. J. Lee, J. Chang, S. Choi, S. Lee, M. Nnaji, X. Liu, and M. Dobrowolska, Sci. Rep. **9**, 1 (2019).
[22] S. Zhao, Z. Zhou, B. Peng, M. Zhu, M. Feng, Q. Yang, Y. Yan, W. Ren, Z. G. Ye, and Y. Liu, Adv. Mater. **29**, 1606478 (2017).
[23] M. Weisheit, S. Fähler, A. Marty, Y. Souche, C. Poinsignon, and D. Givord, Science **315**, 349 (2007).
[24] Y. Wang, X. Zhou, C. Song, Y. Yan, S. Zhou, G. Wang, C. Chen, F. Zeng, and F. Pan, Adv. Mater. **27**, 3196 (2015).
[25] Y. Zhang, W. Zhao, Y. Lakys, J.-O. Klein, J.-V. Kim, D. Ravelosona, and C. Chappert, IEEE Trans. Electron Devices **59**, 819 (2012).
[26] R. Duine, K.-J. Lee, S. S. Parkin, and M. D. Stiles, Nat. Phys. **14**, 217 (2018).
[27] B. Böhm, L. Fallarino, D. Pohl, B. Rellinghaus, K. Nielsch, N. S. Kiselev, and O. Hellwig, Phys. Rev. B **100**, 140411(R) (2019).
[28] X. Zhao, Y. Zhao, W. Liu, Z. Dai, T. Wang, X. Zhao, and Z. Zhang, J. Mater. Sci. Technol. **34**, 832 (2018).
[29] Y.-C. Lau, D. Betto, K. Rode, J. Coey, and P. Stamenov, Nat. Nanotechnol. **11**, 758 (2016).
[30] C. Bi, H. Almasi, K. Price, T. Newhouse-Illige, M. Xu, S. R. Allen, X. Fan, and W. Wang, Phys. Rev. B **95**, 104434 (2017).
[31] K. Wang, Y. Zhang, and G. Xiao, Phys. Rev. Appl. **13**, 064009 (2020).
[32] Y. Zhang, K. Wang, and G. Xiao, Appl. Phys. Lett. **116**, 212404 (2020).
[33] H. X. Yang, M. Chshiev, B. Dieny, J. H. Lee, A. Manchon, and K. H. Shin, Phys. Rev. B **84**, 054401 (2011).
[34] B. Dieny and M. Chshiev, Rev. Mod. Phys. **89**, 025008 (2017).
[35] N. Nagaosa, J. Sinova, S. Onoda, A. H. MacDonald, and N. P. Ong, Rev. Mod. Phys. **82**, 1539 (2010).
[36] K. Wang, L. Qian, W. Chen, S.-C. Ying, G. Xiao, and X. Wu, Phys. Rev. B **99**, 184410 (2019).

[37] See Supplemental Material at http://link.aps.org/supplemental/10.1103/PhysRevB.102.144430 for details on magnetic anisotropies of ferromagnetic layers, atomic-force microscropy, transport, and energy dispersive x-ray spectroscopy measurements, as well as additional results and discussions.
[38] V. Naik, H. Meng, and R. Sbiaa, AIP Adv. **2**, 042182 (2012).
[39] C.-W. Cheng, C. Shiue, T.-I. Cheng, and G. Chern, J. Appl. Phys. **112**, 033917 (2012).
[40] D. Watanabe, S. Mizukami, F. Wu, M. Oogane, H. Naganuma, Y. Ando, and T. Miyazaki, J. Phys. Conf. Ser. **200**, 072104 (2010).
[41] X. Zhang, Y. Zhang, and J. Cai, J. Appl. Phys. **118**, 143903 (2015).
[42] S. S. Kalarickal, X. Y. Xu, K. Lenz, W. Kuch, and K. Baberschke, Phys. Rev. B **75**, 224429 (2007).
[43] S. Schwieger, J. Kienert, K. Lenz, J. Lindner, K. Baberschke, and W. Nolting, Phys. Rev. Lett. **98**, 057205 (2007).
[44] A. L. Yeats, P. J. Mintun, Y. Pan, A. Richardella, B. B. Buckley, N. Samarth, and D. D. Awschalom, Proc. Natl. Acad. Sci. USA **114**, 10379 (2017).
[45] M. S. El Hadri, P. Pirro, C.-H. Lambert, S. Petit-Watelot, Y. Quessab, M. Hehn, F. Montaigne, G. Malinowski, and S. Mangin, Phys. Rev. B **94**, 064412 (2016).
[46] C. Zheng, K. Zhu, S. C. De Freitas, J.-Y. Chang, J. E. Davies, P. Eames, P. P. Freitas, O. Kazakova, C. Kim, and C.-W. Leung, IEEE Trans. Magn. **55**, 1 (2019).